Exploring the Structure of a Photosynthetic Model by Quantum-Chemical Calculations and Time-Resolved Q-Band Electron Paramagnetic Resonance

Andreas M. Kiefer,[†] Stefan M. Kast,[‡] Michael R. Wasielewski,[§] Karl Laukenmann,[†] and Gerd Kothe*,[†]

Contribution from the Department of Physical Chemistry, University of Freiburg, Albertstrasse 21, D-79104 Freiburg, Germany, Department of Physical Chemistry, Darmstadt University of Technology, Petersenstrasse 20, D-64287 Darmstadt, Germany, Chemistry Division, Argonne National Laboratory, 9700 South Cass Avenue, Argonne, Illinois 60439, and Department of Chemistry, Northwestern University, Evanston, Illinois 60208

Received June 2, 1998. Revised Manuscript Received October 13, 1998

Abstract: The structure of the covalent photosynthetic model system *N*,*N*,*N*′,*N*′-tetraalkyl-*p*-phenylenediamine-zinc porphyrin-naphthoquinone (TAPD-ZnP-NQ) has been explored by using a combination of theoretical and experimental techniques. Structural information is extracted from high-level quantum-chemical ab initio calculations, which is a nontrivial task for a large molecule like TAPD-ZnP−NQ. We tackle this problem by dividing the model system into smaller molecular fragments, whose geometries can be optimized separately. The fragments are subsequently fitted together, thus providing an approximate structure of the entire model system. To verify this structure, time-resolved Q-band electron paramagnetic resonance (EPR) experiments on the light-induced radical pair $TAPD^+$ NQ^- have been carried out. The time evolution of the transverse magnetization of $TAPD^+$ NQ^- is monitored at various static magnetic fields. Quantum beat oscillations are observed at early times after the laser pulse. These quantum beats are highly sensitive probes for the geometry of the underlying radical pair. From the good agreement between observed and simulated EPR time profiles we conclude that the ab initio calculations predict the correct geometry within the experimental precision.

Introduction

The light-induced charge separation in photosynthetic reaction centers is one of the most important photochemical reactions known. Despite intensive research in this area, the high quantum yield of this process is still not understood in great detail. One possibility of gaining better insight into this reaction is the use of photosynthetic models, which mimic the function of the reaction centers. These biomimetic complexes can be synthesized with exactly defined donors, bridges, and acceptors and thus allow tuning of specific properties of the electron transfer process. Reviews of this vastly expanding field can be found elsewhere.[1−5] To rationalize the increasing number of results for these systems, structural information is indispensable. However, for most of the photosynthetic models, this presents a major problem since crystals of sufficient size for X-ray crystallography are difficult to obtain. As a result, only limited structural information exists.[6−8]

One of the first effective photosynthetic models to be reported in the literature is the complex *N*,*N*,*N*′,*N*′-tetraalkyl-*p*-phenylenediamine-zinc porphyrin-naphthoquinone (TAPD-ZnP-NQ) (see Figure 1).[9] Optical studies point to the following chain of electron-transfer steps:[9,10]

$$\text{TAPD-ZnP-NQ} \xrightarrow{h\nu} \text{TAPD-}^1\text{ZnP*-NQ} \xrightarrow{5\ \text{ps}} \text{TAPD-ZnP}^+\text{-NQ}^- \xrightarrow{530\ \text{ps}} \text{TAPD}^+\text{-ZnP-NQ}^-$$

After photoexcitation of ZnP, charge separation takes place in 5 ps, forming the primary radical pair, ZnP^+ NQ^-. An electron is then transferred from TAPD to ZnP in 530 ps. The secondary radical pair, $TAPD^+$ NQ^-, is the first intermediate detectable by time-resolved electron paramagnetic resonance (EPR).[11−13]

[†] University of Freiburg.
[‡] Darmstadt University of Technology.
[§] Argonne National Laboratory and Northwestern University.

(1) Gust, D.; Moore, T. A. *Science* **1989**, *244*, 35−41.
(2) Wasielewski, M. R. *Chem. Rev.* **1992**, *92*, 435−461.
(3) Wasielewski, M. R. In *The Photosynthetic Reaction Center*; Deisenhofer, J., Norris, J. R., Eds.; Academic Press: San Diego, 1993; Vol. II, pp 465−511.
(4) Gust, D.; Moore, T. A. In *The Photosynthetic Reaction Center*; Deisenhofer, J., Norris, J. R., Eds.; Academic Press: San Diego, 1993; Vol. II, pp 419−464.
(5) Kurreck, H.; Huber, M. *Angew. Chem., Int. Ed. Engl.* **1995**, *34*, 849−866.
(6) Sessler, J. L.; Johnson, M. R.; Creager, S. E.; Fettinger, J. C.; Ibers, J. A. *J. Am. Chem. Soc.* **1990**, *112*, 9310−9329.
(7) Staab, H. A.; Krieger, C.; Anders, C.; Rückemann, A. *Chem. Ber.* **1994**, *127*, 231−236.
(8) Fajer, J.; Barkgia, K. M.; Melamed, D.; Sweet, R. M.; Kurreck, H.; von Gersdorff, J.; Plato, M.; Rohland, H.-C.; Elger, G.; Möbius, K. *J. Phys. Chem.* **1996**, *100*, 14236−14239.
(9) Wasielewski, M. R.; Gaines, G. L., III; O'Neill, M. P.; Svec, W. A.; Niemczyk, M. P. *J. Am. Chem. Soc.* **1990**, *112*, 4559−4560.
(10) Wasielewski, M. R.; Gaines, G. L., III; O'Neil, M. P.; Niemczyk, M. P.; Svec, W. A. In *Supramolecular Chemistry*; Balzani, V., De Cola, L., Eds.; Kluwer Academic Publishers: Dordrecht, The Netherlands, 1992; pp 201−218.
(11) Laukenmann, K.; Weber, S.; Kothe, G.; Oesterle, C.; Angerhofer, A.; Wasielewski, M. R.; Svec, W. A.; Norris, J. R. *J. Phys. Chem.* **1995**, *99*, 4324−4329.
(12) Van der Est, A. J.; Füchsle, G.; Stehlik, D.; Wasielewski, M. R. *Ber. Bunsen-Ges. Phys. Chem.* **1996**, *100*, 2081−2085.
(13) Van der Est, A. J.; Füchsle, G.; Stehlik, D.; Wasielewski, M. R. *Appl. Magn. Reson.* **1997**, *13*, 317−335.

10.1021/ja981930+ CCC: $18.00
Published on Web 12/19/1998

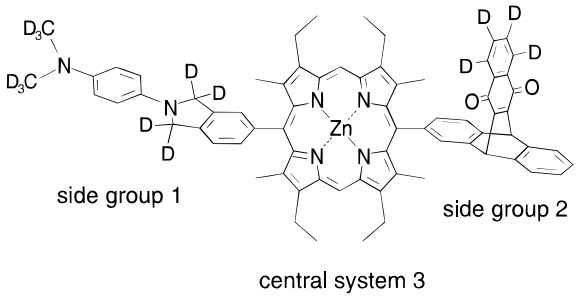

Figure 1. Molecular structure of the partially deuterated (D) photosynthetic model, indicating the three different fragments whose geometry was separately optimized in the ab initio quantum-chemical calculations.

At low temperature, $TAPD^+$ NQ^- stores 1.85 eV of energy for about 4 ms with a quantum yield of 67%.[9,10]

In solid organic glasses, charge separation takes place from an excited singlet state of the primary donor, $^1ZnP^*$. The singlet character is retained during both electron-transfer steps which occur on a fast subnanosecond time scale. Thus, $TAPD^+$ NQ^- is created in a virtually pure singlet state. Since the singlet is not an eigenstate of the corresponding spin Hamiltonian, $TAPD^+$ NQ^- starts out in a coherent superposition of spin states which can manifest itself as quantum beats in an EPR experiment with adequate time resolution (e.g. <50 ns). Previously, we have presented a high time resolution X-band (9.5 GHz) EPR study of $TAPD^+$ NQ^-, formed by photoinduced charge separation at low temperature.[11] Quantum beat oscillations were observed at earlier times after laser pulse excitation.[11]

The frequency of the quantum beats corresponds to the energy separation of specific eigenstates, split by the electron spin−spin interactions and the difference in Zeeman interactions. Under solid state conditions this frequency turns out to be markedly anisotropic, strongly depending on the orientation of the radical pair relative to the static magnetic field. The pronounced anisotropy can be exploited to study the spatial arrangement of the constituent radicals in the charge-separated state. For $TAPD^+$ NQ^-, this geometry is not known with any great detail.[12,13]

In this paper we therefore explore the three-dimensional structure of TAPD-ZnP-NQ by using a combination of theoretical and experimental techniques. First, structural information is extracted from high-level quantum-chemical ab initio calculations, which is a nontrivial task for a large molecule like TAPD-ZnP-NQ. We tackle this problem by dividing the model system into smaller molecular fragments, whose geometry can be optimized separately. The fragments are subsequently fitted together, thus providing an approximate structure of the entire model system.

To verify this structure, time-resolved Q-band (34 GHz) EPR experiments of the light-induced radical pair $TAPD^+$ NQ^- have been carried out. Additional spectral resolution is achieved by employing a partially deuterated model system (see Figure 1). The time evolution of the transverse magnetization of $TAPD^+$ NQ^- is monitored at various static magnetic fields. This implies a two-dimensional variation of the signal intensity with respect to both the magnetic field and the time axis. Quantum beat oscillations are observed at early times after the laser pulse. Analysis of these quantum beats as a function of the static magnetic field is achieved on the basis of the calculated structure. The results indicate that the ab initio calculations predict the correct geometry within experimental precision.

Experimental Section

Sample Preparation. The synthesis of the protonated TAPD-ZnP-NQ model system has been described earlier.[9] Details concerning the preparation of the partially deuterated compound are available from the authors upon request. The material was kept in the dark at 250 K as a dark red powder. Samples for the EPR experiments were always prepared fresh from this stock material. First, the dark red powder was purified under nitrogen atmosphere by using thin-layer chromatography (TLC). The eluting solvent was 95%/5% dichloromethane/acetone (v/v). The second band shows a cherry-red color containing the purified compound. It was scraped off the TLC plate and the compound was extracted from silica gel with acetone. After evaporation of the acetone with a stream of dry nitrogen gas, the pure material was dissolved in ultrapure MTHF (distilled and stored over potassium/sodium alloy). The solution was then filled in an EPR quartz tube of 2 mm inner diameter. After several freeze−pump−thaw cycles, the sample tube was sealed under vacuum. Sample temperature was controlled by a helium flow cryostat (Oxford CF-935) and was stable to within ± 0.2 K.

EPR Measurements. The time-resolved EPR experiments were performed by using a newly developed transient Q-band bridge (Bruker ER 050 QGT) in combination with a Bruker ESP 300 E console. The sample was irradiated in a cylindrical cavity with a loaded Q of approximately 800, corresponding to a bandwidth of 40 MHz. The time resolution of the experimental setup is in the 10 ns range. A Q-band frequency counter (HP 5352 B) was used to monitor the microwave frequency. The magnetic field was calibrated against Si:P, which is an excellent standard for low-temperature measurements.[14]

For optical excitation the frequency-doubled output of a modified Nd:YAG laser (Spectra Physics GCR 130-10) with a wavelength of 532 nm was used. With the short-pulse option we obtained 2.5 ns pulse widths and 280 mJ/pulse output. For the actual experiment the intensity was attenuated to approximately 10 mJ/pulse. To avoid photoselection, the laser beam was passed through a quartz depolarizer. The repetition rate of the laser was 15 Hz. A transient recorder (LeCroy 9354A) with a maximum digitizing rate of 1 ns/11 bit sample was used to aquire the time-dependent EPR signal. A weak zinc porphyrin triplet signal, superimposed on the radical pair signal, was subtracted by using a linear interpolation procedure. Typically, 1200 transients were accumulated at off-resonance conditions and subtracted from those on resonance, to get rid of the laser background signal.

Computations. All ab initio calculations were performed with the Gaussian 92/94 suite of programs[15,16] on a Fujitsu VPP 300/6 (Hessischer Höchstleistungsrechner) at Darmstadt University of Technology. The calculations of the EPR spectra and time profiles were performed with Fortran programs[17] based upon the theoretical approach outlined in Section 4. The corresponding diagonalizations were accomplished by using the Rutishauser algorithm according to Gordon and Messenger.[18] Fortran routines were taken from the literature[18,19] and modified for this purpose.

(14) Stesmans, A.; De Vos, G. *Phys. Rev. B* **1986**, *34*, 6499−6502.

(15) Gaussian 92, Revision F.3, Frisch, M. J.; Trucks, G. W.; Head-Gordon, M.; Gill, P. M. W.; Wong, M. W.; Foresman, J. B.; Johnson, B. G.; Schlegel, H. B.; Robb, M. A.; Replogle, E. S.; Gomperts, R.; Andreas, J. L.; Raghavachari, K.; Binkley, J. S.; Gonzales, C.; Martin, R. L.; Fox, D. J.; Defrees, D. J.; Baker, J.; Stewart, J. J. P.; Pople, J. A. Gaussian Inc.: Pittsburgh, PA, 1992.

(16) Gaussian 94, Revision D.1, Frisch, M. J.; Trucks, G. W.; Schlegel, H. B.; Gill, P. M. W.; Foresman, J. B.; Johnson, B. G.; Robb, M. A.; Cheeseman, J. R.; Keith, T.; Petersson, G. A.; Montgomery, J. A.; Raghavachari, K.; Al-Laham, M. A.; Zakrzewski, V. G.; Ortiz, J. V.; Foresman, J. B.; Cioslowski, J.; Stefanov, B. B.; Nanayakkara, A.; Challacombe, M.; Peng, C. Y.; Chen, W.; Wong, M. W.; Andreas, J. L.; Replogle, E. S.; Gomperts, R.; Martin, R. L.; Fox, D. J.; Binkley, J. S.; Defrees, D. J.; Baker, J.; Stewart, J. J. P.; Head-Gordon, M.; Gonzales, C.; Pople, J. A. Gaussian Inc.: Pittsburgh, PA, 1995.

(17) Laukenmann, K. Ph.D. Thesis, 1999, University of Freiburg.

(18) Gordon, R. G.; Messenger, T. In *Electron Spin Relaxation in Liquids*; Muus, L. T., Atkins, P. W., Eds.; Plenum Press: New York; 1972; pp 341−381.

(19) Cullum, J.; Willoughby, R. A. *Lanczos Algorithms for Large Symmetric Eigenvalue Computations*; Birkhäuser: Basel, 1985; Vol. 2.

Quantum-Chemical Calculations

The determination of the structure of a molecule with more than 500 electrons by means of ab initio methods requires some fragmentation of the molecule. Thus, the photosynthetic model system is divided into smaller molecular fragments whose geometry can be optimized separately. The optimized molecular fragments are subsequently fitted together, yielding the approximate structure of the entire model system. This latter procedure requires a great deal of chemical intuition. The model compound naturally suggests a subdivision into three different molecular fragments: the two side groups 1 and 2 and the central porphyrin system 3 (see Figure 1).

Optimization of the side group fragments has been done on the HF/6-31G* level of theory. In addition, the final conformers of dimethylaniline have been treated including electron correlation with MP2/6-31G*. The central porphyrin unit containing the zinc atom requires the use of effective core potentials; computational details are discussed in greater detail below.

Geometry of Side Group 1. The presence of the two nitrogen atoms in side group 1 introduces a high degree of flexibility, leading in turn to a large number of possible conformers. Consequently, the conformational potential energy surface is very complex and contains a large number of local minima. Global optimization strategies in the context of quantum chemistry with a considerable number of electrons are prohibitive. Hence, we started our calculations on even smaller molecular fragments with an accordingly smaller number of local minima to ultimately infer the global minimum of the entire side group 1 from the topology of locally optimal structures. These smaller fragments include dimethylaniline (DMA), *N*,*N*,*N*,*N*-tetramethyl-*p*-phenylene-diamine (TMPD) and the benzo-annealed *N*,*N*-dialkyl-4-pyrrolidinoaniline (DAPA) (see Figure 2). Since only a small amount of experimental data concerning the structure of DMA or its derivatives exist, theoretical investigations have been carried out in the past.[20−22] The results of our studies are consistent with those investigations in the case of DMA, while no comparable studies are available for TMPD and DAPA discussed later.

DMA was optimized starting from various initial geometries. To classify the conformers obtained from the optimization, two geometry parameters characterizing the position of the nitrogen-bonded methyl groups are introduced (see Figure 2a): (i) the wagging angle θ between the methyl-*N*-methyl plane and the N−C bond, which permits a definition of the inversion barrier for the wagging motion of the nitrogen bonded methyl groups, and (ii) the twist angle α, which defines the amino group rotation around the C−N bond.[20]

If both θ and α are zero the molecule is completely planar and has C_s symmetry. The conformers as obtained from geometry optimization have planar ($\theta = 0°$, $\alpha = 0°$), wagged ($\theta = 26°$, $\alpha = 0°$), twisted ($\theta = 38°$, $\alpha = 43°$), and crossed geometry ($\theta = 43°$, $\alpha = 90°$).[21] The electronic interaction between the nitrogen's lone pair and the delocalized π-electron system of the phenyl ring stabilizes the corresponding geometry position of the amino group. Qualitatively, this effect gets increasingly pronounced in the order crossed < twisted < wagged, corresponding to the energetic order of the MP2 calculations (see Table 1). Although the tendency of delocalization is maximal in the case of the planar conformation, the resulting structure is less favorable because a pyramidalized (sp^3) nitrogen is preferred due to the presence of methyl groups. Therefore, one can conceive the wagged geometry as some kind of compromise structure balancing both opposite effects.[22] The electron correlation, which has not been taken into account in previous investigations,[20−22] is obviously necessary since Hartree−Fock (HF) level theory predicts the twist conformation to be the most favorable one. This is consistent with neither semiempirical results[20] nor chemical intuition.

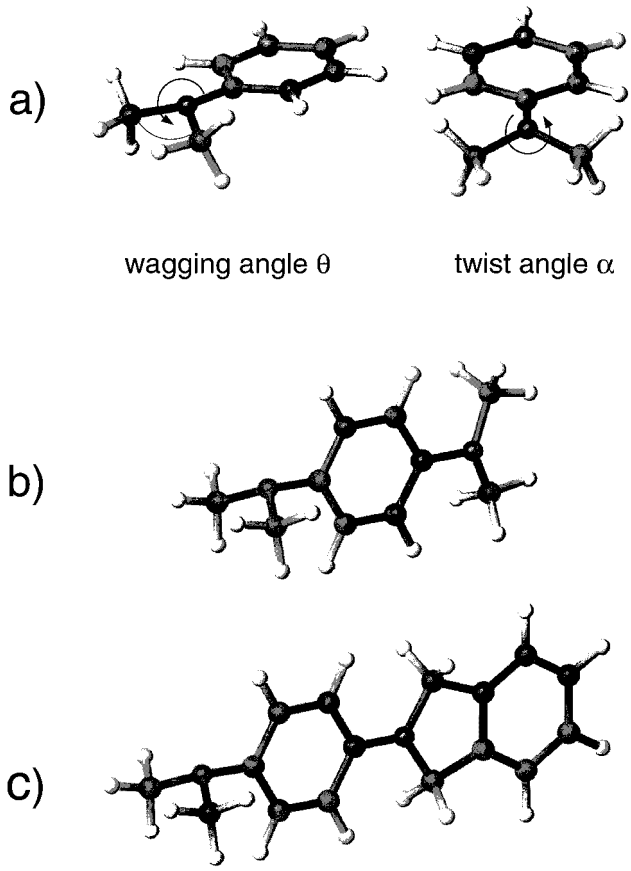

Figure 2. Computed geometries of molecular fragments constituting side group 1. (a) The wagged geometry of *N*,*N*-dimethylaniline (DMA). θ denotes the wagging angle and α is the twist angle. (b) The wagged-crossed geometry of *N*,*N*,*N*,*N*-tetramethyl-*p*-phenylenediamine (TMPD). (c) The crossed-planar geometry of benzo-annealed *N*,*N*-dialkyl-4-pyrrolidino-aniline (DAPA).

The four optimum arrangements of the methyl groups were then taken as starting points for the geometry optimization of the next bigger fragment TMPD (see Figure 2b). In Table 2, the angles and HF energies of the cis and trans isomers of the wagged−wagged and the crossed−crossed conformer are listed. Since the wagging angles of the cis and trans isomers are equal, one can presume that steric effects do not play a major role for the orientation of the methyl groups relative to the benzene ring. In the following, we will therefore refrain from giving details of all possible cis−trans isomers. Comparing the wagging angles with those in DMA, a noticeable change occurs only in the case of the wagged conformers (2 and 5,6) while the crossed conformers (4 and 7,8) are not affected (see Tables 1 and 2). Apparently, this is a consequence of electronic interaction between the nitrogen's lone pair and the delocalized π-electron system of the phenyl ring, which is strong for the wagged conformers but weak for the crossed conformers. Considering only electronic effects leads to 10 different conformers, 8 of which exhibit a minimum in the potential energy surface. They are summarized in Table 3. Note that, for clarity, some conformers appear twice. A noticeable change of the geometry parameters compared to those of DMA arises only if both amino groups interact strongly with the benzene ring: the wagging

(20) Gorse, A.-D.; Pesquer, M. *J. Mol. Struct. (THEOCHEM)* **1993**, *281*, 21−32.

Table 1. Results of Geometry Optimizations (HF/6-31G*) and Single-Point Calculations (MP2/6-31G*) of Dimethylanilin (DMA)[a]

no. of the conformer	position of the amino group	wagging angle θ/deg	twist angle α/deg	$E_{HF/6-31G*}$/ hartree	$E_{MP2/6-31G*}$/ hartree
1	planar	0	0	−363.7796660	−364.9625341
2	wagged	26.2	0	−363.7802385	−364.9638594
3	twisted	38.0	42.6	−364.9638457	−364.9638457
4	crossed	42.7	90.0	−363.7799414	−364.9618137

[a] The geometry is described by the parameters θ and α.

Table 2. Geometry Parameters and Hartree−Fock Energies (HF/6-31G*) of the Cis (C) and Trans (T) Isomers of Wagged−Wagged and Crossed−Crossed *N*,*N*,*N*,*N*-Tetramethyl-*p*-phenylene-diamine (TMPD)

no. of the conformer	position of the amino groups	wagging angle θ/deg	twist angle α/deg	$E_{HF/6-31G*}$/ hartree
5	wagged−wagged^T	31.8	0	−496.8540642
6	wagged−wagged^C	31.8	0	−496.8540452
7	crossed−crossed^T	42.7	90.0	−496.8566819
8	crossed−crossed^C	42.7	90.0	−496.8566153

Table 3. Geometry Parameters and Hartree−Fock Energies (HF/6-31G*) of *N*,*N*,*N*,*N*-Tetramethyl-*p*-phenylene-diamine (TMPD)[a]

no. of the conformer	position of the amino groups	wagging angle θ of the first amino group/deg	twist angle α of the first amino group/deg	$E_{HF/6-31G*}$/hartree
9	planar−planar	0	0	−496.8511985
10	planar−wagged	0	0	−496.8527194
11	planar−crossed	0	0	−496.8559672
12	wagged−planar	33.0	0	−496.8527194
13	wagged−wagged	31.8	0	−496.8540642
14	wagged−crossed	27.1	0	−496.8566390
15	twisted−twisted	39.4	52.6	−496.8576452
16	twisted−crossed	38.4	44.8	−496.8575227
17	crossed−planar	42.4	90.0	−496.8559672
18	crossed−wagged	42.5	90.0	−496.8566390
19	crossed−twisted	42.7	90.0	−496.8575227
20	crossed−crossed	42.7	90.0	−496.8566819

[a] In the case of cis−trans isomerism, only the conformer with the lower energy is listed. Conformers with twisted−planar and twisted−wagged arrangement do not exhibit a minimum in the potential energy surface.

Table 4. Geometry Parameters and Hartree−Fock Energies (HF/6-31G*) of Benzo-Annealed *N*,*N*-Dialkyl-4-pyrrolidinoaniline (DAPA)[a]

no. of the conformer	position of the ring system − position of the amino group	wagging angle θ of the ring system/deg	twist angle α of the ring system/deg	$E_{HF/6-31G*}$/ hartree
21	planar−planar	0	0	−725.2460224
22	planar−wagged	0	0	−725.2475229
23	planar−twisted	0	0	−725.2500766
24	planar−crossed	0	0	−725.2508725
25	wagged−planar	21.2	0	−725.2462854
26	wagged−wagged	19.8	0	−725.2477181
27	wagged−twisted	16.2	0	−725.2501408
28	wagged−crossed	7.3	0	−725.2508763
29	crossed−planar	33.1	90.0	−725.2440943
30	crossed−wagged	31.1	90.0	−725.2447192
31	crossed−twisted	28.6	90.0	−725.2455052
32	crossed−crossed	27.1	90.0	−725.2445508

[a] In case of cis−trans isomerism, only the one with lower energy is listed.

angles of the wagged conformers (12−14) increase with a stronger electronic influence of the additional amino group; the wagging angles of the crossed conformers (17−20) are nearly independent of the position of the opposite amino group.

Shifting our focus to the energies of the conformers, one can see in Table 3 that a strong interaction of both amino groups (e.g. in the case of a planar−planar conformation) leads to a highly unfavorable structure. This is due to the fact that a charge accumulation in the phenyl ring takes place. Conversely, if there is only weak interaction of both amino groups with the phenyl ring (e.g. in the case of a crossed−crossed conformation) the resulting structure is also disadvantaged because of a lack of delocalization. This follows from the structural studies of DMA. One can therefore expect that a minimum energy path connecting the conformers is characterized by the coupled transition from wagged−crossed via twisted−twisted to crossed−wagged, balancing weak and strong electronic delocalization. Only one amino group at a time is electronically coupled to the phenyl ring. The optimum geometries thus closely resemble that of DMA.

The next bigger fragment constitutes the entire side group 1, labeled as DAPA (see Figure 2c). Starting from various initial geometries and ignoring cis−trans isomerism leads to 12 energetically different conformers summarized in Table 4. In contrast to TMPD, no twisted conformations are achieved and the wagging angles of the remaining conformers are much smaller. This is due to the fact that the replacement of two hydrogens by one phenyl ring leads to a charge accumulation on the nitrogen atom, which causes a shift of hybridization from a more sp^3-like state to a more sp^2-like state, increasing planarity.

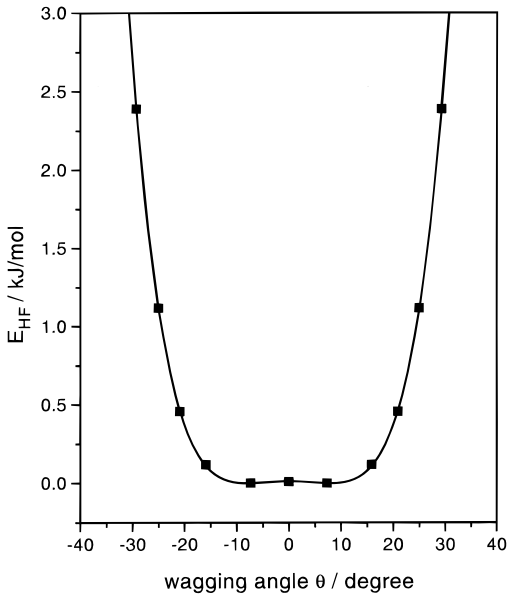

Figure 3. Hartree−Fock energies (HF/6-31G*) for optimized side group 1 as a function of the wagging angle θ of the ring system. The position of the smaller substituent was kept crossed during these calculations. The minimum energy occurs at $\theta = \pm 7.3°$ and the inversion barrier is 0.7 kJ/mol.

This is easily verified by comparing the average energies of the crossed conformers (29−32) with the average energies of the wagged (25−28) and the planar conformers (21−24): the crossed conformers are more than 10 kJ/mol less favorable than the wagged or the planar conformers. This difference in energy and the lack of twisted conformers leads to the conclusion that the ring system of side group 1 has a planar, or slightly wagged position, while the remaining amino group has a crossed, or slightly twisted position. In contrast to TMPD, a coordinated rotation around the angle α of both groups is severely hindered by a large energy barrier that can be attributed to the electronic delocalization over both ring systems.

If the nitrogen-bonded methyl groups of the smaller substituent take a crossed position to the plane of the central phenyl ring, the wagging angle of the bigger substituent is just 7.3° (conformer 28 in Table 4). It is therefore interesting to study the potential energy surface along the reaction pathway wagged−planar−wagged of the bigger substituent. This has been performed on the HF/6-31G* level of theory by varying angles θ of the ring system and keeping the positions of the smaller amino group fixed in a crossed position. As can be seen in Figure 3, a double-well potential is obtained, with a barrier of only 0.7 kJ/mol located at the planar conformation. This barrier is within the range of electron correlation energies, so one cannot be sure whether the inclusion of electron correlation could alter the shape of the potential curve sufficiently to make the planar arrangement more favorable than the wagged conformation. MP2 calculations of the planar and the wagged conformer are beyond the capabilities of computers available to us, so there remain some uncertainties concerning the lowest energy state. However, if there is a barrier between the wagged and the planar conformer, it will be so low that it can be easily passed even under experimental low-temperature conditions. It is thus reasonable to assume a planar conformation on average. Furthermore, one should notice that the five-membered ring in the center of DAPA is not a planar system. A wagging motion does not only affect the DMA part of DAPA as published recently.[12,13] The pentagon behaves like a balance, preventing large deviations from this averaged position of the DMA part.

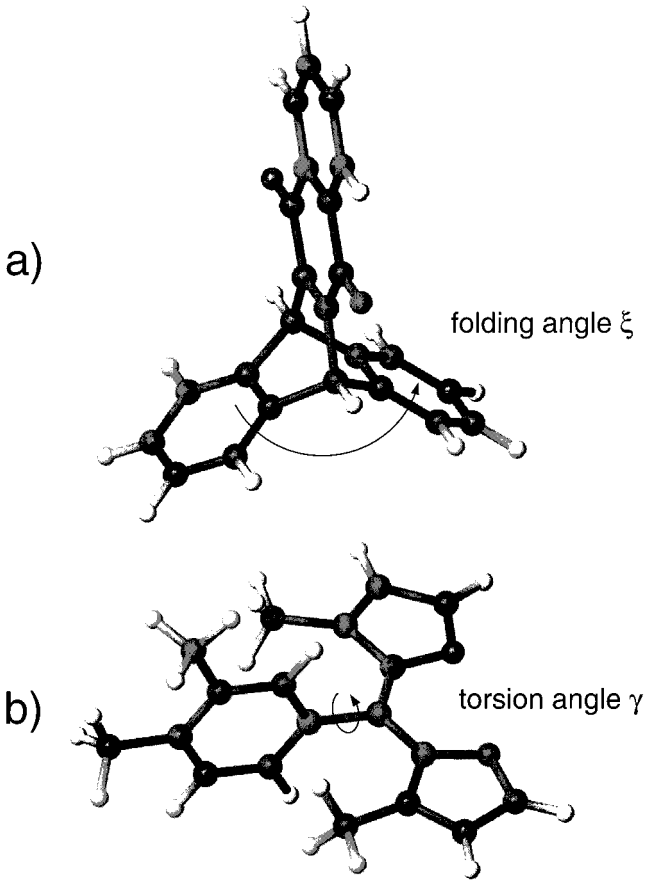

Figure 4. Computed geometries of (a) side group 2 and (b) the connecting unit xylyl-bispyrryl-methylene (XBM). (a) The folding angle amounts to $\xi = 119.3°$ and the corresponding force constant is approximately 417 J/(deg^2 mol). (b) The resulting geometry is characterized by a torsion angle of $\gamma = 90°$ and an associated force constant of 92.4 J/(deg^2 mol).

Hence, even if the position is slightly wagged, the orientation of the donor with respect to the acceptor is not significantly affected.

Side Group 2 and Central Unit. The side group 2 (see Figure 4a) consists of three fairly rigid fragments: one naphthoquinone fragment and two phenyl rings. Only the two sp^3-carbons connecting these three fragments have some degree of flexibility.[23] Hence, the largest amplitude motion of side group 2 is supposedly the libration associated with the folding angle ξ between the planes of the two phenyl rings. The equilibrium angle in the optimized structure is 119.3°. To study the approximate amplitude of this motion, the potential energy surface along the corresponding folding angle was computed with the simpler and therefore less time-consuming molecule triptycene where the naphthoquinone fragment is substituted by a further phenyl ring.[24] The result is a smooth parabola with nearly the same equilibrium angle of 120.0° and a force constant of 417.2 J/(deg^2 mol). A displacement of as little as 3.5° is associated with an energy change of 2.5 kJ/mol. We therefore conclude that the entire side group 2 can be treated as nearly rigid.

The huge number of electrons of the unsubstituted zinc porphyrin prevents all-electron computations on available computer resources, but by using effective core potentials (ECPs) for the transition metal inner shells and by applying symmetry constraints, the required computing time is acceptable. The LANL2DZ basis set[25] combined with a constrained minimum symmetry C_{4v} yields a completely planar porphyrin

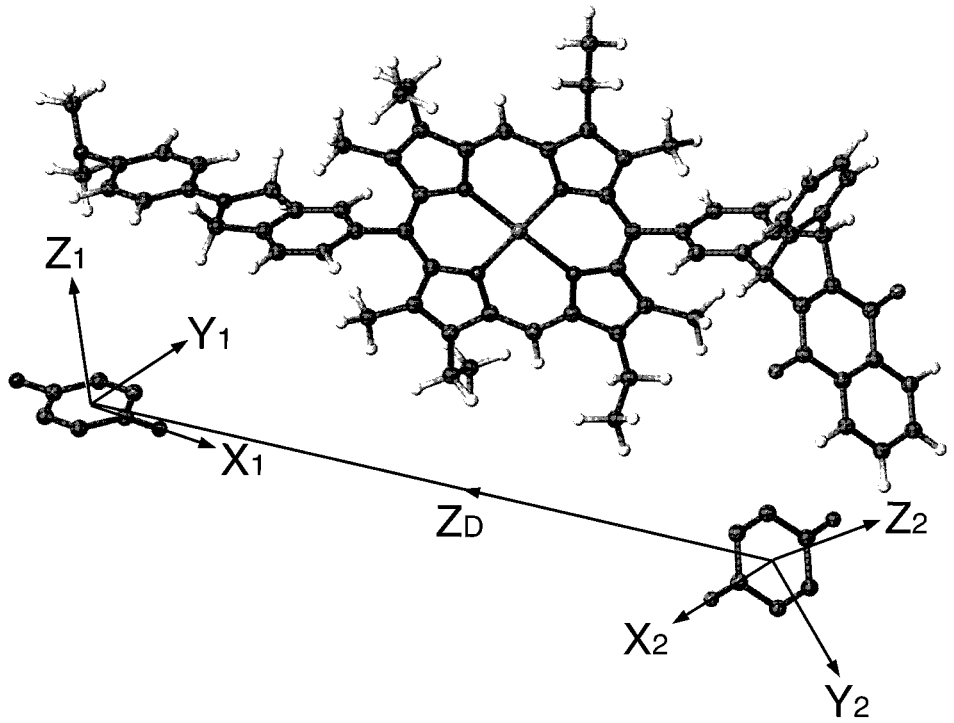

Figure 5. Three-dimensional structure (anti isomer) of the photosynthetic model according to ab initio quantum-chemical calculations. The location and orientation of the magnetic tensors in the secondary radical pair $TAPD^+$ NQ^- are also shown.

system with D_{4h} symmetry. This agrees with porphyrin structures calculated by other groups.[26] The four additional methyl and ethyl groups were then attached to the porphyrin system and optimized separately by using the STO-3G basis set with the macrocyclic system kept rigid. X-ray studies by Fajer et al. indicate a slightly nonplanar porphyrin structure.[27] However, it is not clear whether this deformation is the result of the specific crystal environment. Even if it were the case in the present model system, the deviation from planarity is so small that the effect on the Euler angles entering the EPR simulations would be negligible.

Fragment Linkage. The large number of electrons and the lack of symmetry prevent ab initio calculations of the whole biomimetic molecule. To characterize the torsional degrees of freedom generated by connecting the side groups to the central porphyrin system, a fraction of each side group and a certain model fraction of the central region were constructed, the connecting unit xylyl-bispyrryl-methylidene (XBM) (see Figure 4b). The part approximating the side groups consists of an *o*-xylol system; the part modeling the porphyrin system consists of two connected pyrrole rings and two methyl groups. The atomic positions of the *o*-xylol system were taken from the optimized structures of the side groups; the positions of the connected pyrrole rings were taken from the optimized porphyrin system. The methyl groups were added to the fragment and the geometry was optimized. The resulting structure is characterized by a torsion angle of $\gamma = 90°$ in any case and, by scanning the energetics associated with the torsion, has a force constant of 92.4 J/(deg^2 mol). Thus, a displacement of roughly 7.5° is associated with an energy change of 2.5 kJ/mol.

To study the electronic influence of the model porphyrin fragment on the torsional mode, the two nitrogens were replaced by oxygens. This means that a positive charge instead of a negative one is placed on this fragment. The procedure changes neither the equilibrium angle nor the force constant considerably. This can be attributed to the fact that the two π-electron systems are perpendicularly oriented, so only weak electronic interactions occur. The conformational energy is therefore dominated by steric effects, thus legitimizing the approach taken here.

Three-Dimensional Structure. To obtain the structure of the whole photosynthetic model, the optimized molecular fragments have to be fitted together. This was accomplished by using the program package MOLCAD.[28] According to our fragmentation and assembly strategy, several structural isomers can be constructed. First, there are two isomers associated with the distinct mutual orientation of side group 1 and side group 2, labeled as syn and anti.[13] In addition, the triptycene bridge linking the naphthoquinone to the central system can exist in two stereoisomers, *R* and *L*. By considering our key result, the planar nitrogen of side group 1, *R* and *L* result in enantiomers which cannot be distinguished, neither by quantum chemical calculations nor by EPR. Thus, only two isomers, syn and anti, remain. The corresponding structures are available as PDB files from the authors upon request.

Figure 5 depicts the structure of the anti isomer of the model system. Please note the following characteristic features: One nitrogen of side group 1 is *planar* on average, in contrast to a

(21) Ando, K.; Kato, S. *J. Chem. Phys.* **1991**, *95*, 5966−5982.
(22) Smith, D. A.; Ulmer, C. W., II; Gilbert, M. J. *J. Comput. Chem.* **1992**, *13*, 640−650.
(23) Rosenfeld, S.; Tingle, C. W.; Jasinski, J. P.; Whittum, J. E.; Woudenberg, R. C.; van Epp, J. *J. Am. Chem. Soc.* **1994**, *116*, 12049−12050.
(24) Furlan, A.; Fischer, T.; Fluekiger, P.; Güdel, H.-P.; Leutwyler, S.; Lüthi, H. P.; Riley, M. J.; Weber, J. *J. Phys. Chem.* **1992**, *96*, 10713−10719.
(25) Hay, P. J.; Wadt, W. R. *J. Chem. Phys.* **1985**, *82*, 270−283.
(26) Zwaans, R.; van Lenthe, J. H.; den Boer, D. H. W. *J. Mol. Struct. (THEOCHEM)* **1995**, *339*, 153−160.
(27) Barkigia, K. M.; Berber, D. M.; Fajer, J.; Medforth, C. J.; Renner, M. W.; Smith, K. M. *J. Am. Chem. Soc.* **1990**, *112*, 8851−8857.
(28) Brickmann, J.; Goetze, T.; Heiden, W.; Moeckel, G.; Reiling, S.; Vollhardt, H.; Zachmann, C.-D. In *Insight and Innovation in Data Visualization*; Bowie, J. E., Olson, A. J., Eds.; Addison-Wesley: Reading 1995; pp. 83−97.

recent structural proposal.[12,13] In addition, the zinc porphyrin exhibits a completely planar structure. Distortion of the planarity that may be caused by the attached groups could not be taken into account in the present calculations. The planes of the two benzene rings of side group 2 are orientated at an angle of 119.3°; the fragment is almost completely rigid. Both side groups prefer a perpendicular orientation with respect to the macrocyclic ring, and because of the steric influence of the two methyl groups, large-amplitude fluctuations of the torsion angle are not expected.

Time-Resolved EPR Studies

The primary events of natural and artificial photosynthesis proceed via light-induced radical pairs, generated with correlated spins.[29,30] In this section we present time-resolved Q-band EPR studies for the secondary radical pair, $TAPD^+$ NQ^-, in the photosynthetic model. Particular emphasis is given to quantum beat oscillations[31−33] detectable at early times after laser pulse excitation.[34−36] The quantum beats are highly sensitive probes for the structure of the biomimetic complex.

EPR Model. The total spin Hamiltonian, $H(\Omega)$, depends on the orientation, Ω, of the radical pair and can be divided into five parts:

$$H(\Omega) = H_Z(\Omega) + H_{SS}(\Omega) + H_{HF}(\Omega) + H_{NZ} + H_{MW} \quad (1)$$

In a frame rotating with the microwave frequency, ω, around the static magnetic field, B_0, the first term, describing Zeeman interactions of the electron spins, $\mathbf{S}_i$, $i = 1, 2$, is given by

$$H_Z(\Omega) = \beta B_0(g_1^{zz}(\Omega)S_1^z + g_2^{zz}(\Omega)S_2^z) - \hbar\omega(S_1^z + S_2^z) \quad (2)$$

where β and $g_i^{zz}(\Omega)$ are the Bohr magneton and the zz component of the **g** tensor of radical i, respectively. As usual in the high-field approximation, all nonsecular terms for the electron spins have been neglected. The orientation dependence of $g_i^{zz}(\Omega)$ can be evaluated by a 2-fold transformation from the corresponding principal axis system, in which $\mathbf{g}_i$ is diagonal (g_i^j, $j = X, Y, Z$). In the first step we transform to a molecular reference system (principal axis system of the **g** tensor of NQ^-), using the Euler angles,[37] $\Omega_i = (\Phi_i, \Theta_i, \Psi_i)$, $i = 1, D$. In the second step we rotate by the Euler angles $\Omega = (\Phi, \Theta, \Psi)$ in the laboratory frame.

The second term of the spin Hamiltonian accounts for the spin−spin coupling of the radical pair,

$$H_{SS}(\Omega) = 2(D^{zz}(\Omega) - J_{ex})S_1^zS_2^z - (^1/_2D^{zz}(\Omega) + J_{ex})(S_1^-S_2^+ + S_1^+S_2^-) \quad (3)$$

where J_{ex} and $D^{zz}(\Omega)$ are the strength of the isotropic exchange interaction[38] and the zz component of the dipolar coupling tensor $\mathbf{D}(\Omega)$. Since $\mathbf{D}(\Omega)$ is traceless, two zero-field splitting parameters, D and E, suffice to specify the diagonal tensor.

The third term of the spin Hamiltonian (eq 1) describes the magnetic interactions between electron and nuclear spins. For weakly coupled radical pairs this part of the Hamiltonian can be written as[39]

$$H_{HF}(\Omega) = \sum_k (A_{1k}^{zz}(\Omega)S_1^zI_{1k}^z + B_{1k}(\Omega)S_1^zI_{1k}^x) + \sum_l (A_{2l}^{zz}(\Omega)S_2^zI_{2l}^z + B_{2l}(\Omega)S_2^zI_{2l}^x) \quad (4)$$

where $\mathbf{I}_{ik}$ is the spin operator of nucleus k in radical i. A_{ik}^{zz} and B_{ik} denote the secular and pseudosecular part of the hyperfine interactions between nucleus k and radical i, specified by the principal values A_{ik}^j, $j = X, Y, Z$, of the corresponding diagonal tensor.

The nuclei, in addition, experience Zeeman interactions. Thus, the fourth term of the spin Hamiltonian may be written as

$$H_{NZ} = \sum_k -\beta_n g_{1k}B_0I_{1k}^z + \sum_l -\beta_n g_{2l}B_0I_{2l}^z \quad (5)$$

where β_n denotes the nuclear Bohr magneton and g_{ik} is the g-factor for nucleus k in radical i.

In the presence of a microwave field assigned to the x-axis of the rotating frame, the Hamiltonian includes the radiation term:

$$H_{MW} = {}^1/_2(g_1 + g_2)\beta B_1(S_1^x + S_2^x) \quad (6)$$

Here, g_i is the isotropic g-factor of radical i and B_1 denotes the magnitude of the microwave radiation.

Having specified the spin Hamiltonian, we now discuss the initial configuration of the spin pair immediately after the laser flash. In the photosynthetic model TAPD-ZnP-NQ the secondary radical pair, $TAPD^+$ NQ^-, is generated in a virtually pure singlet state.[9,10] This implies formation of zero quantum electron coherence[31−36] and single quantum nuclear coherence[40−43] between specific eigenstates of the radical pair. In the absence of a microwave field, the eigenstate populations are constant in time, while the zero quantum electron coherences oscillate at distinct frequencies, ω_{ZQ}, given by the energy separation of the corresponding eigenstates:[36]

$$\omega_{ZQ} = (1/\hbar)\{[^2/_3D^{zz}(\Omega) - 2J_{ex}]^2 + [(g_1^{zz}(\Omega) - g_2^{zz}(\Omega))\beta B_0 + \sum_k A_{1k}^{zz}(\Omega)M^i{}_{1k} - \sum_l A_{2l}^{zz}(\Omega)M_{2l}^j]^2\}^{1/2} \quad (7)$$

$$M^{\mathbf{i}}_{1k} = I_{1k}, I_{1k} - 1, ..., -I_{1k} \quad (8)$$

$$M_{2l}^j = I_{2l}, I_{2l} - 1, ..., -I_{2l} \quad (9)$$

In deriving eqs 7−9 all pseudosecular terms of the hyperfine interactions have been neglected. As a result, light-generated

(29) Closs, G. L.; Forbes, M. D. E.; Norris, J. R. *J. Phys. Chem.* **1987**, *91*, 3592−3599.
(30) Buckley, C. D.; Hunter, D. A.; Hore, P. J.; McLauchlan, K. H. *Chem. Phys. Lett.* **1987**, *135*, 307−312.
(31) Salikhov, K. M.; Bock, C. H.; Stehlik, D. *Appl. Magn. Reson.* **1990**, *1*, 195−211.
(32) Bittl, R.; Kothe, G. *Chem. Phys. Lett.* **1991**, *177*, 547−553.
(33) Zwanenburg, G.; Hore, P. J. *Chem. Phys. Lett.* **1993**, *203*, 65−74.
(34) Kothe, G.; Weber, S.; Bittl, R.; Ohmes, E.; Thurnauer, M. C.; Norris, J. R. *Chem. Phys. Lett.* **1991**, *186*, 474−480.
(35) Kothe, G.; Weber, S.; Bittl, R.; Norris, J. R.; Snyder, S. S.; Tang, J.; Thurnauer, M. C.; Morris, A. L.; Rustandi, R. R.; Wang, Z. In *Spin Chemistry*; I'Haya, Y. J., Ed.; The Oji International Conference on Spin Chemistry: Tokyo, 1991; pp 420−434.
(36) Kothe, G.; Weber, S.; Ohmes, E.; Thurnauer, M. C.; Norris, J. R. *J. Phys. Chem.* **1994**, *98*, 2706−2712.
(37) Edmonds, A. R. *Angular Momentum in Quantum Mechanics*; Princeton University Press: Princeton, 1974; pp 6−8.
(38) The sign of the exchange interaction parameter, J_{ex}, has been chosen according to common practice.
(39) Reitz, D. C.; Weissman, S. I. *J. Chem. Phys.* **1960**, *33*, 700−704.
(40) Weber, S.; Ohmes, E.; Thurnauer, M. C.; Norris, J. R.; Kothe, G. *Proc. Natl. Acad. Sci. U.S.A.* **1995**, *92*, 7789−7793.
(41) Weber, S.; Kothe, G.; Norris, J. R. *J. Chem. Phys.* **1997**, *106*, 6248−6261.
(42) Kothe, G.; Bechtold, M.; Link, G.; Ohmes, E.; Weidner, J.-U. *Chem. Phys. Lett.* **1998**, *283*, 51−60.
(43) Jeschke, G. J. *Chem. Phys.* **1997**, *106*, 10072−10086.

nuclear coherences[41−43] are not considered in the analysis. The same is true for nuclear coherences, created by the microwave radiation.[41,44]

The continuous microwave field, applied in transient EPR, has two effects. First, it converts the longitudinal magnetization associated with the population differences between neighboring eigenstates into transverse magnetization.[33,45] This gives the Torrey oscillations,

$$\omega_{TO} \approx {}^1/_2(g_1 + g_2)\beta B_1/\hbar \qquad (10)$$

virtually independent of B_0.[33,45] Second, it converts the zero quantum electron coherence into observable single quantum precessions or quantum beats,[31−36] significantly varying with B_0.[32,34,36] Yet, the conventional transient EPR experiment does not give the frequency of the zero quantum precession directly because the coherence transfer, required to observe this precession, is modulated by Torrey oscillations.[33]

Under solid-state conditions, the frequency of the quantum beats critically depends on the orientation of the radical pair in the laboratory frame (see eq 7). The weak B_1 field, commonly employed in transient EPR, allows for only a small range of orientations to meet the resonance condition. Consequently, the phase and frequency of the quantum beats varies significantly with B_0 across the powder spectrum. This pronounced variation can be used to extract the geometry of radical pair intermediates in photosynthetic reaction centers.[34,36,46]

Experimental Data. Generally, a complete EPR data set consists of transient signals taken at equidistant field points covering the total spectral width. This yields a two-dimensional variation of the signal intensity with respect to both the magnetic field and the time axis. Such a complete data set measured at a microwave frequency of $\omega/2\pi$=33.8766 GHz (Q-band) is shown in Figure 6. The plot refers to the partially deuterated model system, a microwave field of $B_1 = 0.036$ mT and $T = 30$ K. Note that a positive signal indicates absorptive (a) and a negative emissive (e) spin polarization. Transient spectra can be extracted from this plot at any fixed time after the laser pulse as slices parallel to the magnetic field axis. Likewise, the time evolution of the transverse magnetization may be obtained for any given field as a slice along the time axis. In the following, transient spectra and time profiles are discussed separately.

It is obvious from Figure 6 that the line shapes vary significantly with time. Generally, the early spectra are much broader than the later ones. Moreover, the polarization changes from a simple e/a pattern at early times (<30 ns) to a characteristic e/a/e/a pattern at later times. A typical line shape, observed 130 ns after the laser pulse, is shown in Figure 7. The spectrum refers to a microwave field of $B_1 = 0.036$ mT and $T = 30$ K. Approximately the same e/a/e/a polarization pattern was observed over an intermediate time range, extending from 100 to 150 ns. It can be assigned to the charge-separated state, $TAPD^+$ NQ^-, of the secondary radical pair.

Figure 8 depicts the time evolution of the transverse magnetization of $TAPD^+$ NQ^-, measured at two different field positions (C and E, Figure 7). The transients refer to a microwave field of $B_1 = 0.053$ mT and $T = 30$ K. Apparently, there are fast initial oscillations which disappear 100 ns after the laser pulse. In addition, slow persisting oscillations with a frequency of 1.4−1.5 MHz can be observed. Basically, these slow oscillations represent Torrey precessions whose frequency is linearly dependent on the applied microwave magnetic field (see eq 10). From the decay of these transient nutations, the

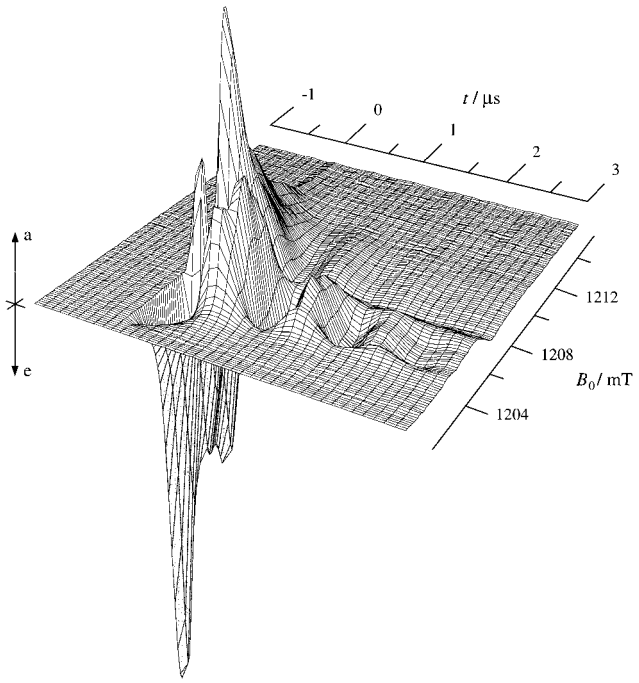

Figure 6. Complete Q-band data set of the transient EPR signal of the light-induced radical pair $TAPD^+$ NQ^- in the partially deuterated model system. Positive and negative signals indicate absorptive (a) and emissive (e) polarizations, respectively. Microwave field, $B_1 = 0.036$ mT. Microwave frequency, $\omega/2\pi = 33.8766$ GHz. Temperature, $T = 30$ K.

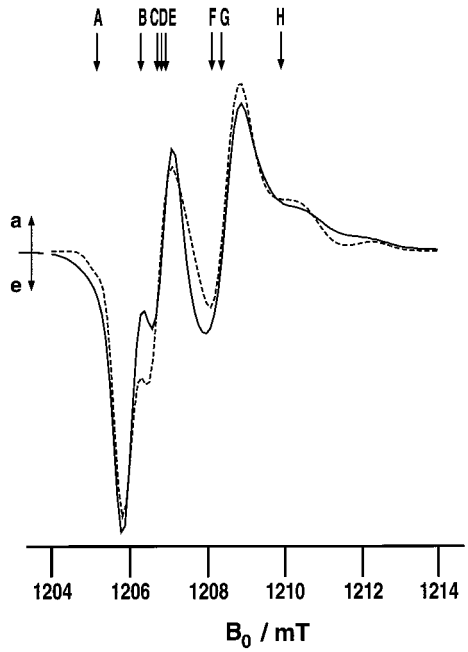

Figure 7. Transient Q-band EPR spectrum of the light-induced radical pair $TAPD^+$ NQ^- observed 130 ns after the laser pulse. Positive and negative signals indicate absorptive (a) and emissive (e) polarizations, respectively. Microwave field, $B_1 = 0.036$ mT. Microwave frequency, $\omega/2\pi = 33.8766$ GHz. Full line: experimental spectrum from the partially deuterated model system. Temperature, $T = 30$ K. Dashed line: calculated spectrum using the parameters given in Tables 5 and 6. Various field positions are marked from A to H. The time evolution of the transverse magnetization at those field positions is shown in the Figures 8−10.

(44) Jeschke, G.; Schweiger, A. *Mol. Phys.* **1996**, *88*, 335−383.
(45) Gierer, M.; van der Est, A.; Stehlik, D. *Chem. Phys. Lett.* **1991**, *186*, 238−247.
(46) Kothe, G.; Weber, S.; Ohmes, E.; Thurnauer, M. C.; Norris, J. R. *J. Am. Chem. Soc.* **1994**, *116*, 7729−7734.

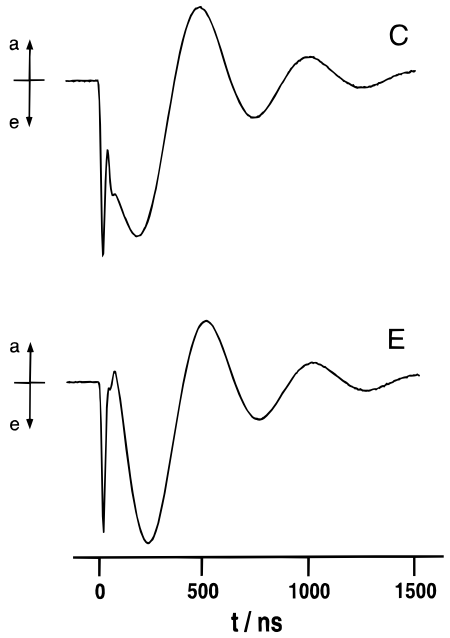

Figure 8. Q-band EPR time profiles for the light-induced radical pair $TAPD^+$ NQ^- at two different static magnetic fields (positions C and E, Figure 7). Positive and negative signals indicate absorptive (a) and emissive (e) polarizations, respectively. Microwave field, $B_1 = 0.053$ mT. Microwave frequency, $\omega/2\pi = 33.8766$ GHz. Temperature, $T =$ 30 K.

homogeneous spin−spin relaxation time, T_2, can be estimated.[47] The T_2 values of $TAPD^+$ NQ^- vary significantly across the powder spectrum from $T_2 \approx 300$ ns at position B to $T_2 \approx 150$ ns at position H. Observation of Torrey oscillations requires underdamping conditions,[48] i.e., $\omega_{TO} \gg 1/T_2$, which are generally satisfied for $B_1 = 0.053$ mT. In case of a lower microwave power, however, overdamping behavior is expected primarily at the high-field wing of the spectrum, in agreement with the experimental observations (see Figure 6).

Interestingly, the frequency of the fast initial oscillations is independent of the microwave power but changes with the magnetic field position. Figures 9 and 10 depict the short time behavior of the transverse magnetization measured at eight selected field positions (A−H, Figure 7). All transients refer to a constant microwave field of $B_1 = 0.053$ mT and $T = 30$ K. Note that these initial oscillations vary significantly across the powder spectrum. Generally, oscillation frequencies from 15 to 52 MHz can be extracted from the corresponding power spectra, obtained by Fourier transformation of the time profiles. Up to now, these fast initial oscillations of the transverse magnetization have not been observed at Q-band frequency. Basically, they represent quantum beats associated with the spin-correlated generation of the radical pair (see eqs 7−9).

Simulations. Analysis of the Q-band EPR experiments of $TAPD^+$ NQ^- was performed by employing the EPR model outlined above. Table 5 summarizes the magnetic and structural parameters used in the calculations. The **g** tensor components of $TAPD^+$, g_1^i, $i = X, Y, Z$, were estimated on the basis of the isotropic *g*-factor, measured for the isolated TMPD radical cation.[49] Approximate values for the **g** tensor of NQ^-, g_2^i, $i = X, Y, Z$, could be obtained from the partially relaxed Q-band EPR spectrum of $TAPD^+$ NQ^-.[17] Generally, the $\mathbf{g}_2$ tensor components are significantly larger than those determined for the 2,3-dimethyl-1,4-naphthoquinone (DMNQ) radical anion.[50] Interestingly, similar high g^i values have been reported for the first quinone acceptor in photosystem II.[51]

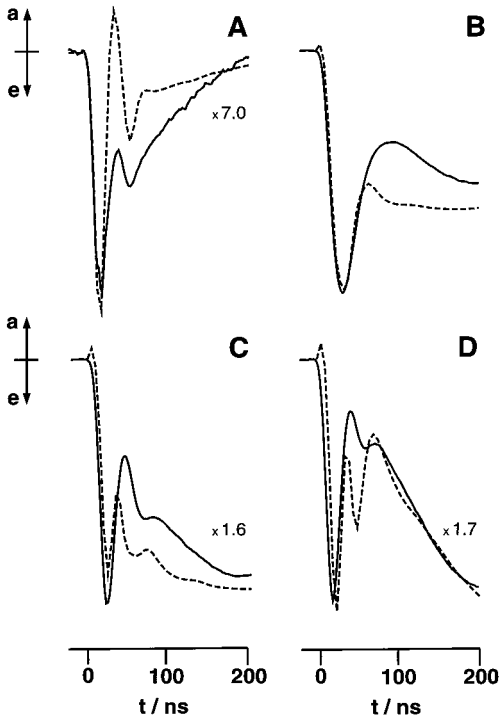

Figure 9. Time evolution of the transverse magnetization of the light-induced radical pair $TAPD^+$ NQ^- immediately after the laser pulse. The transients refer to four different static magnetic fields (positions A−D, Figure 7). Positive and negative signals indicate absorptive (a) and emissive (e) polarizations, respectively. Microwave field, $B_1 =$ 0.053 mT. Microwave frequency, $\omega/2\pi = 33.8766$ GHz. Full lines: experimental time profiles from the partially deuterated model system. Temperature, $T = 30$ K. Dashed lines: calculated time profiles using the parameters given in Tables 5 and 6.

By using a point dipole approximation,[52] the parameters of the dipolar coupling tensor, *D* and *E*, were estimated on the basis of the calculated structure. Values of $D = -0.28$ and -0.26 mT for the syn and anti isomer favorably compare with $D = -0.29$ mT, evaluated from the electron spin−echo envelope modulation (ESEEM) of $TAPD^+$ NQ^-.[17] The ESEEM study also provided an estimate for the exchange interaction parameter of $J_{ex} = +0.23$ mT,[17] in substantial agreement with recent K-band investigations with liquid crystals.[12,13] The exchange coupling in $TAPD^+$ NQ^- is at least 2 orders of magnitude larger than that found in the analogous radical pairs of photosynthetic reaction centers.

Angles for the magnetic tensor orientations in $TAPD^+$ NQ^- were extracted from the calculated structure of the model system (see Figure 5). The listed Euler angles[37] relate the principal axis system of the respective magnetic tensor (**g** tensor of $TAPD^+$, dipolar coupling tensor) and the molecular reference system, collinear with the **g** tensor of NQ^-.[53] Hyperfine interactions in the partially deuterated model system were considered by using published nitrogen and proton hyperfine tensors for $TAPD^+$ and

(47) Furrer, R.; Fujara, F.; Lange, C.; Stehlik, D.; Vieth, H. M.; Vollmann, W. *Chem. Phys. Lett.* **1980**, *75*, 332−339.
(48) Torrey, H. C. *Phys. Rev.* **1949**, *76*, 1059−1068.
(49) Falle, H. R.; Luckhurst, G. R. *J. Magn. Reson.* **1970**, *3*, 161−199.
(50) Burghaus, O.; Plato, M.; Rohrer, M.; Möbius, K.; MacMillan, F.; Lubitz, W. *J. Phys. Chem.* **1993**, *97*, 7639−7647.
(51) MacMillan, F.; Lendzian, F.; Renger, G.; Lubitz, W. *Biochemistry* **1995**, *34*, 8144−8156.
(52) Coffmann, R. E.; Beuttner, G. R. *J. Phys. Chem.* **1979**, *83*, 2387−2392.
(53) Hales, B. F. J. A. *Chem. Soc.* **1975**, *97*, 5993−5997.

Table 5. Magnetic and Structural Parameters Used in the Calculation of Transient EPR Experiments of the Light-Induced Radical Pair $TAPD^+$ NQ^- in the Partially Deuterated Photosynthetic Model

g tensor components[a]		spin−spin coupling[b]		$\mathbf{g}_1$ tensor orientation[c]		dipolar tensor orientation[c]	
$TAPD^+$	NQ^-	anti	syn	anti	syn	anti	syn
g_1^X, 2.0030	g_2^X, 2.0071	D, −0.26 mT	D, −0.28 mT	Φ_1, 0°	Φ_1, 60°	Φ_D, arbitr	Φ_D, arbitr
g_1^Y, 2.0030	g_2^Y, 2.0055	E, 0	E, 0	Θ_1, 60°	Θ_1, 120°	Θ_D, 40°	Θ_D, 48°
g_1^Z, 2.0023	g_2^Z, 2.0023	J_{ex}, +0.23 mT	J_{ex}, +0.23 mT	Ψ_1, 270°	Ψ_1, 90°	Ψ_D, 63°	Ψ_D, 43°

[a] Data for $TAPD^+$ assumed on the basis of the measured isotropic g-factor.[49] Data for NQ^- evaluated from the partially relaxed Q-band EPR spectrum of $TAPD^+$ NQ^-.[17] [b] D and E values estimated on the basis of the calculated structure. J_{ex} value from a recent ESEEM study of $TAPD^+$ NQ^-.[17] [c] The Euler angles[37] are extracted from the calculated structure. They relate the principal axis system of the respective magnetic tensor and the molecular reference system (**g** tensor of NQ^-).[53]

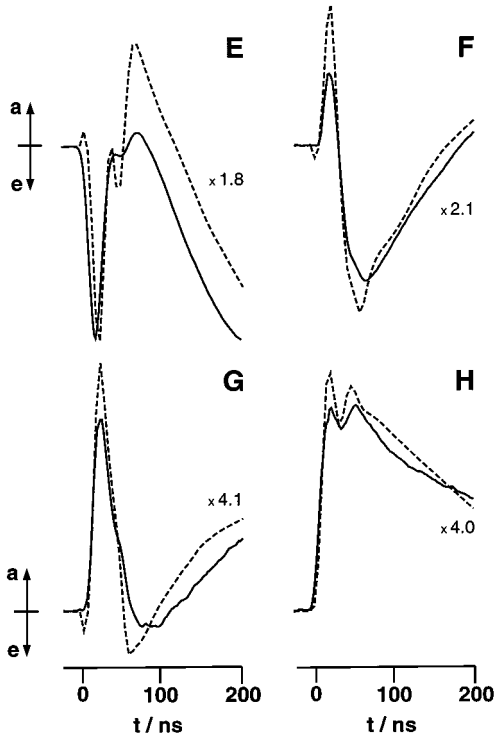

Figure 10. Time evolution of the transverse magnetization of the light-induced radical pair $TAPD^+$ NQ^- immediately after the laser pulse. The transients refer to four different static magnetic fields (positions E−H, Figure 7). Positive and negative signals indicate absorptive (a) and emissive (e) polarizations, respectively. Microwave field, $B_1 = 0.053$ mT. Microwave frequency, $\omega/2\pi = 33.8766$ GHz. Full lines: experimental time profiles from the partially deuterated model system. Temperature, $T = 30$ K. Dashed lines: calculated time profiles using the parameters given in Tables 5 and 6.

Table 6. Hyperfine Interaction Parameters Used in the Calculation of Transient EPR Experiments of the Light-Induced Radical Pair $TAPD^+$ NQ^- in the Partially Deuterated Photosynthetic Model

hyperfine interactions			
in $TAPD^+$ [a,b]			in NQ^- [a,b]
^{14}N nuclei (2)	methyl deuterons (10)	phenyl protons (4)	aliphatic protons (2)
A_{1N}^X, + 0.55 mT	A_{1D}^X, + 0.10 mT	A_{1H}^X, − 0.244 mT	A_{2H}^X, + 0.20 mT
A_{1N}^Y, + 0.55 mT	A_{1D}^Y, + 0.10 mT	A_{1H}^Y, − 0.052 mT	A_{2H}^Y, + 0.20 mT
A_{1N}^Z, + 1.78 mT	A_{1D}^Z, + 0.10 mT	A_{1H}^Z, − 0.300 mT	A_{2H}^Z, + 0.20 mT

[a] Data from an ENDOR study in liquid crystals.[54] The hyperfine tensors in $TAPD^+$ are assumed to be collinear with the corresponding **g** tensor. [b] Residual hyperfine interactions are considered by convolution with a Gaussian of line width ΔB_0=0.2 mT.

$DMNQ^-$.[54] The corresponding parameters are summarized in Table 6. Note that the ^{14}N and ^{1}H hyperfine tensors in $TAPD^+$ were assumed to be collinear with the corresponding **g** tensor. Residual hyperfine interactions were considered by convolution with a Gaussian of line width $\Delta B_0 = 0.2$ mT.

Typically, 3072 grid points, regularly spaced over the surface of a sphere, were employed to simulate the static distribution of the radical pair with respect to the laboratory frame. In Figure 7 we compare the experimental (full line) and calculated (dashed line) Q-band EPR spectrum of $TAPD^+$ NQ^- taken 130 ns after light excitation. The calculated line shape is the sum over the two isomers syn and anti. Inspection reveals minor deviations between the experimental and calculated spectrum. These may be due to uncertainties in the employed magnetic parameters for $TAPD^+$. W-band EPR and X-band ESEEM could provide the necessary information. Studies along these lines, involving a deuterated and ^{15}N substituted model system, are currently in progress.

Analysis of the Q-band EPR spectrum reveals that the low-field e/a polarization pattern is a contribution to the line shape from NQ^-. In contrast, the broad e/a signal from $TAPD^+$ shows up as two distinct shoulders in the high-field absorptive wing of the spectrum. For the X-band EPR spectrum of $TAPD^+$ NQ^- a similar assignment has been proposed,[11] but was questioned in later publications.[12,13] Yet, the present high-resolution Q-band study strongly supports the previous assignment.

In Figures 9 and 10 we compare experimental (solid lines) and calculated time profiles (dashed lines) at early times after light excitation. In the calculations, the limited bandwidth of the cavity was considered by using a band-pass filter at 40 MHz. In addition, spin relaxation was considered by multiplying each time profile by an exponential decay curve, characterized by the corresponding spin−spin relaxation time T_2. Generally, the calculated time profiles compare favorably with their experimental counterparts. In particular, the phase and frequency of the quantum beats and their dependence on the static magnetic field is faithfully reproduced by the calculations. Thus, we conclude that the geometry for $TAPD^+$ NQ^-, evaluated on the basis of ab initio calculations, is basically correct.

Discussion

Solution Structure. Quantum-chemical calculations yield the structure of the photosynthetic model system in the gas phase. The experimental situation is of course different, since the biomimetic molecule is located in a solvent matrix. On the other hand, simulations of the time profiles, based on the calculated geometry, are in reasonable agreement with their experimental counterparts. This at first surprising result can be rationalized by considering the potential contact between solvent molecules and complex. Figure 11 depicts the solvent accessible surface of the photosynthetic model, calculated with a Conolly algorithm.[55] In this method, the solvent molecule is approximated by a sphere of appropriate diameter and rolled over the surface

(54) Kirste, B. *Magn. Reson. Chem.* **1987**, *25*, 166−175.

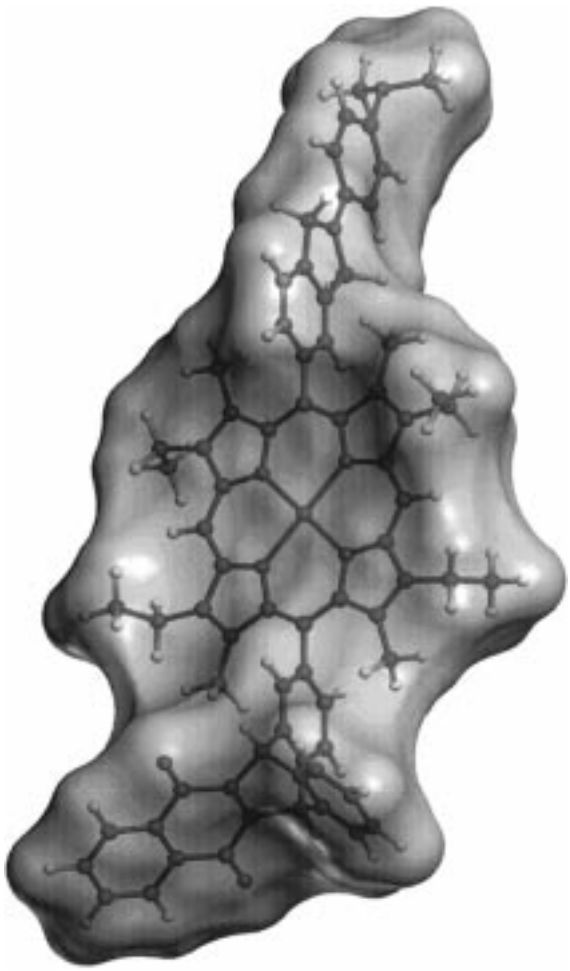

Figure 11. Solvent accessible surface of the photosynthetic model system, indicating the closest contact between the MTHF molecules and the biomimetic complex.

of the solute, whose shape is represented by the van der Waal's radii of the atoms. The resulting contact surface indicates the closest contact between the MTHF molecules and the photosynthetic model. As can be seen in Figure 11, the solvent is unable to occupy the space between the side groups and the macrocyclic ring. We therefore expect that the solvent has practically no effect on the relative orientation of the side groups, in agreement with the above findings.

On the other hand, the presence of a solvent will certainly affect the solute's structure and energetics. With increasing computer power and an appropriately parametrized continuum model for MTHF, it will be possible to treat the structure in solution to a first-order approximation by means of self-consistent reaction field methods in the future.[56,57] We are well aware that we only treated the ground-state geometry of the model system in our ab initio calculations. Accurate computations of the charge-separated state are at present technically out of the question. However, the experimental conditions (covalent model system, low temperature) do not allow for large geometrical changes between the ground-state and the charge-separated state. As emphasized by our results, the ground-state calculations provide a reliable representation of the real structure.

Quantum Beat Oscillations. Generally, the agreement between the experimental time profiles and their calculated counterparts is good. Nevertheless, some deviations still exist. In principle, these deviations may be caused by nuclear modulations observed in the transverse magnetization of the radical pair.[11,17] Because of the enormous computational effort, these nuclear modulations were not considered in the present calculations (see eqs 7−9). So far, two distinct mechanisms have been proposed as the origin of these modulations. The first modulation scheme[41−43] arises from nuclear coherence generated by the laser pulse, which is then transferred to transverse electron magnetization by the continuous microwave magnetic field. In the second mechanism,[41,44] the modulations are both created and detected by the continuous microwave radiation. It appears that the second mechanism is most consistent with experimental observations at high microwave power.[41,44] In the case of low B_1 fields, however, both mechanisms contribute to the observed nuclear modulations.[42]

Notably, the modulation depth of the light-induced nuclear coherences turns out to be low at Q-band frequency.[42] Similar is true for nuclear modulations, created by the microwave radiation.[41,44] Apparently, the higher B_0 field employed in Q-band studies has the advantage of effectively suppressing nuclear modulations, observed at X-band frequency. Moreover, the anisotropy of the quantum beat oscillations is considerably increased, providing a higher orientation selectivity. Thus, it appears that Q-band quantum beats represent excellent structural probes for the short-lived intermediates in the primary energy conversion steps of natural and artificial photosynthesis.

Acknowledgment. This research was financially supported by the Deutsche Forschungsgemeinschaft. Research at ANL and Northwestern University was supported by the Division of Chemical Sciences, Office of Basic Energy Sciences, U.S. Department of Energy, under contract W-31-109-Eng-38. A.M.K thanks Matthias Keil for assistance in the computations and Dr. Dirk Harryvan and Ulrich Heinen for many helpful discussions. Three-dimensional structural model plots were produced with MOLCAD.

JA981930+

(55) Conolly, M. L. *Science* **1983**, *221*, 709−713.
(56) Miertus, S.; Tomasi, J. *Chem. Phys.* **1982**, *65*, 239−245.
(57) Wong, M. W.; Wiberg, K. B.; Frisch, M. J. *J. Am. Chem. Soc.* **1992**, *114*, 523−529.